J. Fluid Mech. (2014), *vol.* 738, *pp.* 358–377. © Cambridge University Press 2013
doi:10.1017/jfm.2013.598

Geostrophic adjustment in a closed basin with islands

E. R. Johnson[1],† **and R. H. J. Grimshaw**[2]

[1]Department of Mathematics, University College London, Gower Street, London WC1E 6BT, UK
[2]Department of Mathematical Sciences, Loughborough University, LE11 3TU, UK

(Received 1 May 2013; revised 29 September 2013; accepted 7 November 2013;
first published online 5 December 2013)

We consider the geostrophic adjustment of a density-stratified fluid in a basin of constant depth on an f-plane in the context of linearized theory. For a single vertical mode, the equations are equivalent to those for a linearized shallow-water theory for a homogeneous fluid. Associated with any initial state there is a unique steady geostrophically adjusted component of the flow compatible with the initial conditions. This steady component gives the time average of the flow and is analogous to the adjusted flow in an unbounded domain without islands. The remainder of the response consists of superinertial Poincaré and subinertial Kelvin wave modes and expressions for the energy partition between the modes in arbitrary basins again follow directly from the initial conditions. The solution for an arbitrary initial density distribution released from rest in a circular domain is found in closed form. When the Rossby radius is much smaller than the basin radius, appropriate for the baroclinic modes, the interior adjusted solution is close to that of the initial state, except for small-amplitude trapped Poincaré waves, while Kelvin waves propagate around the boundaries, carrying, without change of form, the deviation of the initial height field from its average.

Key words: stratified flows, topographic effects, waves in rotating fluids

1. Introduction

Geostrophic adjustment occurs in a rotating fluid when an initial state relaxes to a steady state in geostrophic balance. In the linearized theory for open systems, the adjustment typically occurs by the generation of the waves allowed by the system, which propagate to infinity, and leave a steady state determined by geostrophic equilibrium and the conservation of potential vorticity (see for instance Gill (1982) amongst many works on this topic). For instance, in a long shallow channel filled with a fluid of constant density, the adjustment takes place through Poincaré and Kelvin waves (see Gill 1976). However, in a closed system, the adjustment takes a different form since the generated waves cannot escape to infinity, and hence the flow does not become steady, and consists for all time of both waves and the geostrophically balanced steady component. This situation arises for instance in lakes, where due to the density stratification, the response to temporally localized wind forcing is typically the generation of internal Poincaré and Kelvin waves, together

† Email address for correspondence: e.johnson@ucl.ac.uk

https://doi.org/10.1017/jfm.2013.598 Published online by Cambridge University Press

with a steady component (see, for instance, Stocker & Imberger (2003), Wake *et al.* (2004, 2005) and Wake, Hopfinger & Ivey (2007) and Gomez-Giraldo, Imberger & Antenucci (2006) for a combination of theory, numerical simulations, observations and experiments).

This present study is motivated by the recent numerical and theoretical study by Luneva, Willmott & Maqueda (2012) on geostrophic adjustment in the Arctic Ocean. They considered a homogeneous fluid in a circular basin, with idealized topography, and showed that after the Poincaré and Kelvin waves have been damped by friction, the flow adjusts to a quasi-steady state. Here we consider the adjustment of a density-stratified fluid in a constant-depth basin allowing for islands within the basin (and, later, gaps in the basin boundary) so that any qualitative differences due to the presence of features such as the Canadian Archipelago and the open boundaries of the Arctic Ocean are retained. In this case, the governing equations for a single vertical mode are equivalent to the linearized shallow-water equations for a homogeneous fluid of constant depth on an f-plane. This latter case was discussed by Stocker & Imberger (2003) for a linear initial tilt of the free surface, and as expected the solution consisted of Poincaré and Kelvin waves, and a steady geostrophic component. Here, after presenting the general theory for arbitrary initial states, we put a special emphasis on the limit when the Rossby radius is much smaller than the basin radius. For the baroclinic vertical modes, this is the expected normal situation. Timmermans *et al.* (2010) observed stratifications in the Canada Basin of the Arctic Ocean where the ratio of buoyancy frequency to Coriolis parameter is almost constant and close to two over a significant fraction of the water column, giving a first baroclinic deformation radius of approximately 10 km. We show that the flow is then dominated by the steady geostrophic component and boundary-trapped Kelvin waves.

In § 2 we formulate the problem and obtain the governing equations for the unique steady geostrophic component and the energy partition between the wave modes. Then in § 3 we take the explicit example of a circular basin, revisit the free waves first discussed by Lamb (1932) and formally present the full solution as a Laplace transform. It transpires that it is simpler to solve the full problem numerically and these results are presented in § 3.3. In § 4 we return to considering domains of arbitrary shape with interior islands and boundary gaps and show how our results apply in the limit when the Rossby radius is much smaller than typical geometric dimensions. We conclude in § 5 by noting a simple application to estimate the strength of the Southern Mode oscillation in the Antarctic Circumpolar current for general wind stress curl.

2. Formulation

We consider an incompressible, inviscid density-stratified fluid with basic density $\rho_0(z)$ bounded above by a free surface at $z=\zeta$ and below by a rigid boundary at $z=-H$, contained in a basin $\mathscr{D}$, with outer vertical boundary $\partial\mathscr{D}_0$, possibly containing islands also with vertical boundaries $\partial\mathscr{D}_i$ $(i=1,2,\ldots)$ (figure 1). Then the linearized long-wave equations on an f-plane are, in conventional notation,

$$u_x+v_y+w_z=0, \tag{2.1a}$$

$$\rho_0(u_t-fv)+p_x=0, \tag{2.1b}$$

$$\rho_0(v_t+fu)+p_y=0, \tag{2.1c}$$

$$p_z+g\rho=0, \tag{2.1d}$$

$$\rho_t+\rho_{0z}w=0. \tag{2.1e}$$

https://doi.org/10.1017/jfm.2013.598 Published online by Cambridge University Press

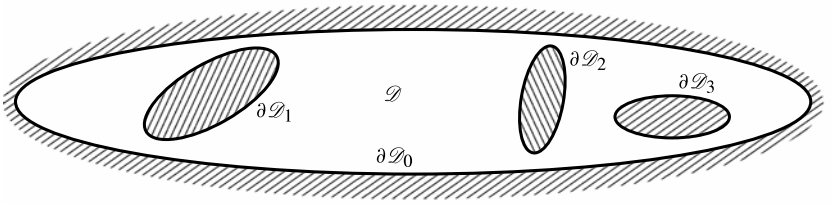


FIGURE 1. The basin $\mathscr{D}$ with outer boundary $\partial\mathscr{D}_0$ and possible islands with boundaries $\partial\mathscr{D}_i$ $(i = 1, 2, \ldots)$.

Here p, ρ are the perturbation pressure and density, respectively. The boundary conditions are

$$\zeta_t - w = 0, \quad z = 0, \tag{2.2a}$$

$$p - g\rho_0\zeta = 0 \quad z = 0, \tag{2.2b}$$

$$w = 0, \quad z = -H \tag{2.2c}$$

$$\boldsymbol{u}\cdot\hat{\boldsymbol{n}} = 0 \quad \text{on } \partial\mathscr{D}, \tag{2.2d}$$

where $\partial\mathscr{D} = \partial\mathscr{D}_0 \cup \partial\mathscr{D}_1 \cup \cdots$, and, for definiteness, $\hat{\boldsymbol{n}}$ is the unit inward normal for $\mathscr{D}$. It is now useful to introduce the vertical particle displacement η. In the linearized theory this is defined by

$$\eta_t = w. \tag{2.3}$$

Then note that $\eta(z = 0) = \zeta$ and the density equation (2.1*e*) integrates to

$$\rho = -\rho_{0z}\eta. \tag{2.4}$$

A solution of this system of equation and boundary conditions can now be sought using separation of variables (see Gill 1982 for instance). That is, we write

$$\eta = \tilde{\eta}(x, y, t)\phi(z), \quad (u, v) = (\tilde{u}, \tilde{v})(x, y, t)h\phi_z(z), \quad p = \tilde{\eta}(x, y, t)c^2\rho_0(z)\phi_z(z). \tag{2.5}$$

Here c^2, h are separation constants which will be specified below. Then the modal function $\phi(z)$ satisfies the boundary value problem

$$c^2(\rho_0\phi_z)_z - g\rho_{0z}\phi = 0, \quad -H < z < 0, \tag{2.6a}$$

$$c^2\phi_z = g\phi, \quad z = 0 \quad \text{and} \quad \phi = 0, \quad z = -H. \tag{2.6b}$$

Here c is the linear long wave speed. In general, there are infinitely many solutions, which can be ordered by an index m, so that ϕ_0, c_0 is the barotropic mode and ϕ_m, c_m, $(m = 1, 2, \ldots)$ are the baroclinic modes, ordered so that the c_m decrease as m increases. We fix attention on just one mode, and then find that

$$\tilde{\eta}_t + h(\tilde{u}_x + \tilde{v}_y) = 0, \tag{2.7a}$$

$$h(\tilde{u}_t - f\tilde{v}) + c^2\tilde{\eta}_x = 0, \tag{2.7b}$$

$$h(\tilde{v}_t + f\tilde{u}) + c^2\tilde{\eta}_y = 0. \tag{2.7c}$$

This system can now be recognized as the linearized shallow-water equations with equivalent depth h defined by setting $c^2 = gh$. We remove the $\tilde{}$ from η, u, v, and note that (2.7*b*) and (2.7*c*) allow boundary condition (2.2*d*) to be written

$$\frac{\partial^2\eta}{\partial n\partial t} - f\frac{\partial\eta}{\partial s} = 0 \quad \text{on } \partial\mathscr{D}, (t > 0), \tag{2.8}$$

https://doi.org/10.1017/jfm.2013.598 Published online by Cambridge University Press

where s is a displacement around each $\partial\mathscr{D}_i$ such that $(\hat{\boldsymbol{z}}, \hat{\boldsymbol{n}}, \hat{\boldsymbol{s}})$ forms a right-handed system. This definition reflects the fact that, for $f > 0$, Kelvin waves cycle anticlockwise around the inside of the outer boundary $\partial\mathscr{D}_0$ but clockwise around the island boundaries $\partial\mathscr{D}_1, \partial\mathscr{D}_2, \ldots$. Adding d$x$ times (2.7*a*) to dy times (2.7*b*), integrating around each boundary and using (2.2*d*) shows that the boundary and island circulations

$$\Gamma_i = \oint_{\partial\mathscr{D}_i} (u\,\mathrm{d}x + v\,\mathrm{d}y), \quad (i = 0, 1, 2, \ldots), \tag{2.9}$$

are constants of the motion. In the absence of initial conditions, these are traditionally arbitrarily set to zero in steady ocean models (e.g. Kamenkovich 1961) but here are determined directly by the initial conditions.

The governing equations are to be solved for the evolution of an initially unbalanced flow given by

$$\eta = \eta_I(x, y), \quad u = u_I(x, y), \quad v = v_I(x, y) \quad \text{at } t = 0. \tag{2.10}$$

These initial conditions immediately determine the circulations Γ_i from (2.9) with u_I, v_I substituted for u, v. For the Gill (1982) problem of a unbalanced density distribution released from rest, or for initial conditions that have been set up conservatively from rest, the Γ_i vanish identically, as they do in the periodically forced wave scattering problems of Rhines (1969) and Johnson (1989). However, for the adjustment of an arbitrary current system (Rossby 1938), or one set up non-conservatively from rest, the Γ_i are generally non-zero, as expected (since otherwise non-zero around-island circulations would not be observed). Equations (2.7) give the potential vorticity equation

$$v_{xt} - u_{yt} - (f/h)\eta_t = 0, \tag{2.11}$$

which integrates to

$$v_x - u_y - f\eta/h = \Pi_I(x, y); \quad \Pi_I = v_{Ix} - u_{Iy} - (f/h)\eta_I \quad (t > 0), \tag{2.12}$$

where the initial conditions (2.10) determine the potential vorticity, Π_I, of each mode for all $t > 0$.

2.1. *The geostrophic mode*

In an unbounded flow without islands, equation (2.12) allows the final steady adjusted state to be obtained directly without intermediate solution of the temporal development. However, in general for a bounded domain or a domain with one or more islands, a non-decaying wavefield co-exists for all time with the steady component of the flow. Nevertheless it remains possible to pose a closed problem for the unique steady adjusted component of the flow, denoted here by $\eta_S(x, y)$, that is consistent with the initial conditions and gives the long-time average of the flow. For steady flow, equations (2.7*b*) and (2.7*c*) give the geostrophic relations

$$u = -(g/f)\eta_y, \quad v = (g/f)\eta_x, \tag{2.13}$$

and (2.12) becomes the inhomogeneous modified Helmholtz equation

$$\nabla^2\eta - K^2\eta = -K^2\eta_I + K(v_{Ix} - u_{Iy}), \tag{2.14}$$

where horizontal distances have been scaled on L, a typical basin scale, speeds on c, η on h and $K = fL/c$ is a Kelvin number measuring the basin scale in Rossby radii and also giving the number of inertial periods required for a Kelvin wave to cycle the

https://doi.org/10.1017/jfm.2013.598 Published online by Cambridge University Press

basin. Note that $a = 1/K$ is the Rossby radius non-dimensionalized on the basin scale. Equation (2.14) is to be solved subject to the boundary conditions, from (2.8), that

$$\eta = \alpha_i \quad \text{on } \partial\mathscr{D}_i, \quad (i = 0, 1, 2, \ldots), \tag{2.15}$$

where the constants α_i give the time-averaged interface displacements at the boundaries and remain to be determined. Since the solution η_S of this boundary-value problem yields, from (2.13), a streamfunction for the adjusted component of the flow, the difference between the α_i values on two boundaries gives the time-averaged mass flux between those boundaries. When no island is present, α_0 follows immediately from the conservation of mass,

$$\int_{\mathscr{D}} \eta = M = \int_{\mathscr{D}} \eta_I, \tag{2.16}$$

for M a constant determined by the initial conditions. When islands are present substituting (2.13) in (2.9) gives

$$\oint_{\partial\mathscr{D}_i} \frac{\partial \eta}{\partial n}\,\mathrm{d}s = \Gamma_i = \oint_{\partial\mathscr{D}_i} (u_I\,\mathrm{d}x + v_I\,\mathrm{d}y), \quad (i = 0, 1, 2, \ldots). \tag{2.17}$$

For rigid-lid flows (where $K = 0$ and neither Poincaré nor Kelvin waves are present) the circulation conditions (2.17) are sufficient to determine a unique solution of (2.14) subject to (2.15) (Lin 1941). A slight modification of the argument for rigid-lid steady flow with $K = 0$ in Kamenkovich (1961) allows us to show straightforwardly that these conditions remain sufficient to determine uniquely the steady adjusted component compatible with the initial conditions when $K \neq 0$ and, in a further slight departure from Kamenkovich (1961), that it is not necessary that the Γ_i vanish identically.

Let η_{S0} be the unique solution of the inhomogeneous equation (2.14) subject to the homogeneous boundary conditions that η_{S0} vanishes on each $\partial\mathscr{D}_i$, and let $\eta^{(j)} (j = 0, 1, 2, \ldots)$ be the unique solutions of the homogeneous form of (2.14) (with $\Pi_I = 0$) subject to the boundary conditions

$$\eta^{(j)} = 1 \quad \text{on } \partial\mathscr{D}_j, \quad \eta^{(j)} = 0 \quad \text{on } \partial\mathscr{D}_i, \quad (i \neq j), (i, j = 0, 1, 2, \ldots), \tag{2.18}$$

so that associated with each $\eta^{(j)}$ are the island circulations

$$G_{ij} = \oint_{\partial\mathscr{D}_i} \frac{\partial \eta^{(j)}}{\partial n}\,\mathrm{d}s. \tag{2.19}$$

The steady adjusted component is then given by the sum

$$\eta_S = \eta_{S0} + \sum_j \alpha_j \eta^{(j)}, \tag{2.20}$$

with the α_j to be determined. Substituting (2.20) in (2.17) gives the matrix equation

$$\boldsymbol{G\alpha} = \boldsymbol{\Gamma}, \tag{2.21}$$

for $\boldsymbol{G} = \{G_{ij}\}$, $\boldsymbol{\alpha} = \{\alpha_j\}$, $\boldsymbol{\Gamma} = \{\hat{\Gamma}_i\}$, where

$$\hat{\Gamma}_i = \Gamma_i - \oint_{\partial\mathscr{D}_i} \frac{\partial \eta_{S0}}{\partial n}\,\mathrm{d}s. \tag{2.22}$$

Provided that $\boldsymbol{G}$ is non-singular the unknown island interface displacements, and hence the solution (2.20), are uniquely determined by (2.21). This follows most directly by

https://doi.org/10.1017/jfm.2013.598 Published online by Cambridge University Press

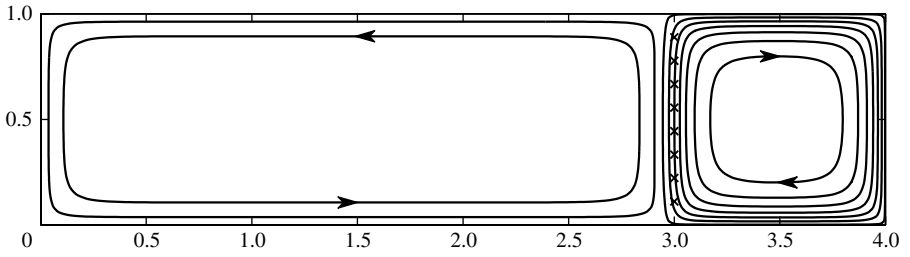


FIGURE 2. The geostrophic mode when $K = 10$ for the release from rest of the initial displacement $\eta_I = \mathrm{sgn}(x - 3)$. The line of the initial surface discontinuity is marked by crosses and the arrows show the direction of the gyre circulations.

showing that $\boldsymbol{\alpha} = 0$ is the unique solution of (2.21) when $\boldsymbol{\Gamma} = 0$. Let $\hat{\eta}$ be a solution of the homogeneous form of (2.14) subject to (2.15) with α_i arbitrary and (2.17) with each Γ_i zero. Then

$$\int_{\mathscr{D}} (|\nabla\hat{\eta}|^2 + K^2\hat{\eta}^2) = -\int_{\mathscr{D}} \hat{\eta}(\nabla^2\hat{\eta} - K^2\hat{\eta}) + \oint_{\partial\mathscr{D}} \hat{\eta}\frac{\partial\hat{\eta}}{\partial n}\,\mathrm{d}s = 0. \tag{2.23}$$

The first integral on the right-hand side vanishes as $\hat{\eta}$ satisfies (2.14) (with $\Pi_I = 0$) and the second since

$$\oint_{\partial\mathscr{D}_i} \hat{\eta}\frac{\partial\hat{\eta}}{\partial n}\,\mathrm{d}s = \alpha_i \oint_{\partial\mathscr{D}_i} \frac{\partial\hat{\eta}}{\partial n}\,\mathrm{d}s = \alpha_i\Gamma_i = 0, \tag{2.24}$$

since $\boldsymbol{\Gamma} = 0$. Thus, $\hat{\eta}$ vanishes identically in $\mathscr{D}$ and so $\boldsymbol{\alpha} = 0$ as required.

With increasing K the diagonal elements of $\boldsymbol{\Gamma}$ dominate as the free-surface deformation isolates the dynamics near each island, so $\alpha_i \to \hat{\Gamma}_i/G_{ii}$. Figure 2 shows the geostrophic mode in a rectangular basin, computed by solving (2.14) and (2.21) using double Chebyshev expansions, excited when the surface $\eta_I = \mathrm{sgn}(x - 3)$ is released from rest. The velocity tangential to the basin boundary in each of the two gyres is approximately constant and so, in order to satisfy the zero-circulation constraint for flows released from rest, the strength of each gyre varies approximately inversely as the length of its perimeter along the basin boundary. This unequal gyre strength is absent from the work of Stocker & Imberger (2003), Wake *et al.* (2005) and Luneva *et al.* (2012) due to the symmetry of their initial conditions.

The general form of η_S for adjustment from rest in a circular domain without islands is given in § 3 and the form of η_S for an arbitrary domain at large Kelvin number is discussed in § 4.

2.2. *The Poincaré and Kelvin wavefields*

Eliminating u, v from (2.12) using (2.7) gives the inhomogeneous Klein–Gordon equation,

$$\eta_{tt} + K^2\eta - \nabla^2\eta = \Pi_I, \tag{2.25}$$

which governs the complete evolution, subject to the initial conditions (2.10). Here t has been scaled on L/c, the time for a Kelvin wave to cycle the basin. Subtracting the steady geostrophic component then leaves the wavefield satisfying the homogeneous form of (2.25) (with $\Pi_I = 0$) subject to (2.8). Each component of the wavefield has zero circulation around the boundaries and amplitude determined by the initial

https://doi.org/10.1017/jfm.2013.598 Published online by Cambridge University Press

conditions. Explicit expressions for the wave mode amplitudes follow directly from the energy product introduced by Proudman (1929). Thus, let the (non-dimensional) normal solutions of (2.7) be denumerable (for $m = 0, 1, 2, 3, \ldots$) as

$$(u, v, \eta) = \mathrm{Re}\{u_m(x, y)\exp(-\mathrm{i}\omega_m t), v_m(x, y)\exp(-\mathrm{i}\omega_m t), \eta_m(x, y)\exp(-\mathrm{i}\omega_m t)\}, \quad (2.26)$$

and introduce the complex vector $\boldsymbol{q}_m = (u_m, v_m, \eta_m)$ with inner product and associated energy norm

$$\langle \boldsymbol{q}_m, \boldsymbol{q}_n \rangle = \int_{\mathscr{D}} (u_m \bar{u}_n + v_m \bar{v}_n + \eta_m \bar{\eta}_n), \quad (2.27a)$$

$$\|\boldsymbol{q}_m\|^2 = \langle \boldsymbol{q}_m, \boldsymbol{q}_m \rangle = \int_{\mathscr{D}} (|u_m|^2 + |v_m|^2 + |\eta_m|^2), \quad (2.27b)$$

where the overbar denotes the complex conjugate. Here $\|\boldsymbol{q}_m\|^2$ is the conserved total energy associated with mode m throughout the evolution with $|\eta_m|^2$ giving the local potential energy and

$$|u_m|^2 + |v_m|^2 = [(K^2 + \omega_m^2)|\nabla \eta_m|^2 + \omega_m \mathrm{Im}\, \partial(\eta_m, \bar{\eta}_m)]/(K^2 - \omega_m^2)^2, \quad (2.28)$$

giving (from (2.7*b*) and (2.7*c*) with $\partial(\eta_m, \bar{\eta}_m)$ the Jacobian) the local kinetic energy, and reducing to the usual expression for the geostrophic mode when $\omega_m = 0$. Here we have assumed that ω_m is real-valued, which is readily shown as follows: take the system satisfied by $\boldsymbol{q}_m$, multiply by $\bar{\boldsymbol{q}}_m$, integrate over $\mathscr{D}$ and subtract the conjugate to give

$$(\omega_m - \bar{\omega}_m)\|\boldsymbol{q}_m\|^2 = 0, \quad (2.29)$$

showing that the ω_m are real. Next, take the system satisfied by $\boldsymbol{q}_m$, multiply by $\bar{\boldsymbol{q}}_n$, integrate over $\mathscr{D}$ and subtract the conjugate, to give

$$(\omega_m - \omega_n)\langle \boldsymbol{q}_m, \boldsymbol{q}_n \rangle = 0, \quad (2.30)$$

showing that modes corresponding to distinct eigenvalues are orthogonal under the inner product (2.27*a*). Moreover, equation (2.30) shows that the geostrophic component $\boldsymbol{q}_S(x, y)$ (say), with frequency $\omega = 0$, is orthogonal to all wave modes. Since an orthogonal basis can be constructed for distinct modes corresponding to repeated eigenvalues, the flow evolution can be postulated to be of the form

$$\boldsymbol{q}(x, y, t) = \boldsymbol{q}_S + \sum A_m \boldsymbol{q}_m \exp(-\mathrm{i}\omega_m t), \quad (t > 0), \quad (2.31)$$

where the modal amplitudes are determined from the initial conditions, $\boldsymbol{q}_I(x, y) = \boldsymbol{q}(x, y, 0)$, as

$$A_m = \langle \boldsymbol{q}_m, \boldsymbol{q}_I - \boldsymbol{q}_S \rangle / \|\boldsymbol{q}_m\|^2 = \langle \boldsymbol{q}_m, \boldsymbol{q}_I \rangle / \|\boldsymbol{q}_m\|^2. \quad (2.32)$$

The norm of (2.31) gives

$$\|\boldsymbol{q}\|^2 = \|\boldsymbol{q}_I\|^2 = \|\boldsymbol{q}_S\|^2 + \sum |A_m|^2 \|\boldsymbol{q}_m\|^2, \quad (t > 0), \quad (2.33)$$

with the energy in each wavemode determined immediately by the projection of the initial state onto the mode independently of the adjusted geostrophic mode. It has not been possible to show that the expansion (2.31) is complete for arbitrary initial conditions and domains. However, equation (2.33) allows the accuracy of the expansion to be computed in the energy norm. In the examples presented below for circular domains the solution, found as a Laplace transform in § 3.2, is complete.

https://doi.org/10.1017/jfm.2013.598 Published online by Cambridge University Press

3. A circular basin without islands

For fluid released from rest in a circular basin of radius L the initial elevation and the solution can be expressed in polar coordinates as a sum of azimuthal modes,

$$\eta_I(r,\theta)=\sum_{-\infty}^{\infty}\eta_{In}(r)\exp(\mathrm{i}n\theta),\quad \eta(r,\theta,t)=\sum_{-\infty}^{\infty}\eta_n(r,t)\exp(\mathrm{i}n\theta) \tag{3.1}$$

with each mode satisfying, from (2.25), (2.8) and (2.10),

$$\eta_{nrr}+(1/r)\eta_{nr}-(n^2/r^2)\eta_n-\eta_{ntt}-K^2\eta_n=-K^2\eta_{In}, \tag{3.2a}$$

$$r\eta_{nrt}+\mathrm{i}nK\eta_n=0\quad\text{at } r=1. \tag{3.2b}$$

$$\eta_n=\eta_{In}(r),\quad \eta_{nt}=0\quad\text{at } t=0. \tag{3.2c}$$

3.1. *Free waves*

First, we examine the free wave modes, as in Lamb (1932). Thus, we set $\eta_{nI}=0$ and seek solutions for which

$$\eta_n(r,t)=F_n(r)\exp(-\mathrm{i}\omega t). \tag{3.3}$$

The solution of (3.2*a*) of form (3.3) that is smooth at $r=0$ is

$$F_n(r)=\mathrm{J}_n(\kappa r)\quad\text{where } \kappa^2=\omega^2-K^2. \tag{3.4}$$

The boundary condition then gives

$$\omega\kappa\mathrm{J}_n'(\kappa)-nK\mathrm{J}_n(\kappa)=0. \tag{3.5}$$

This determines ω as a function of K and the transverse wavenumber n. For each n there is a countable infinity of Poincaré wave solutions, all superinertial, that is $\kappa^2=\omega^2-K^2>0$. When $n\neq 0$, there is also a single subinertial mode where $\kappa^2=-\gamma^2<0$, which can be identified as a Kelvin wave. We then replace (3.4) and (3.5) with

$$\eta=\mathrm{I}_n(\gamma r)\quad\text{where } \gamma^2=K^2-\omega^2. \tag{3.6a}$$

$$\omega\gamma\mathrm{I}_n'(\gamma)-nK\mathrm{I}_n(\gamma)=0,\quad n=1,2,\ldots. \tag{3.6b}$$

The dispersion relation (3.5) can be solved numerically, or graphically as by Lamb (1932). When $n=0$, the only solutions are the superinertial Poincaré waves with $\kappa=j_{s0}'$, the zeros of J_0', indexed by $s=1,2,3,\ldots$, and so

$$\omega^2=K^2+j_{s0}'^2. \tag{3.7}$$

For $n\neq 0$ it is sufficient to consider only $n=1,2,3,\ldots$, as the case $n<0$ is recovered by replacing ω with $-\omega$. Likewise we can take $K>0$ (for the northern hemisphere) without loss of generality, as $K<0$ is also recovered by replacing ω with $-\omega$. Let

$$\Phi(\kappa)=\kappa\mathrm{J}_n'(\kappa)/n\mathrm{J}_n(\kappa)=1-\kappa\mathrm{J}_{n+1}(\kappa)/n\mathrm{J}_n(\kappa), \tag{3.8}$$

and the dispersion relation becomes

$$K/\omega=\pm K/(K^2+\kappa^2)^{1/2}=\Phi(\kappa). \tag{3.9}$$

Here the alternate signs correspond to $\omega>0,<0$, respectively. Note that when $\kappa\to 0$, $\Phi(\kappa)\approx 1-\kappa^2/2n(n+1)$. Otherwise $\Phi\to\pm\infty$ as $\kappa\to j_{sn}$, the zeros of $\mathrm{J}_n(\kappa)$, and $\Phi=0$ at $\kappa=j_{sn}'$, the zeros of $\mathrm{J}_n'(\kappa)$, where for each fixed n, $j_{sn}'<j_{sn}$.

https://doi.org/10.1017/jfm.2013.598 Published online by Cambridge University Press

s	$+1$	$+2$	$+3$	-1	-2	-3
$n=1$	1.51	5.39	8.58	−2.35	−5.46	−8.61
$n=2$	1.93	6.59	9.91	−2.80	−6.64	−9.92

TABLE 1. Frequencies ω for $n=1,2$ and $s=\pm1,\pm2,\pm3$ when $K=1$.

Consequently, $\Phi(\kappa)$ varies from 1 to $-\infty$ in $0<\kappa<j_{1n}$ passing through zero at $\kappa=j'_{1n}$, then from ∞ to $-\infty$ in $j_{1n}<\kappa<j_{2n}$, passing through 0 at $\kappa=j'_{2n}$ and so on. There are clearly then an infinite number of intercepts with the left-hand side K/ω, one with $\omega<0$ in each interval $j'_{sn}<\kappa<j_{sn}$ and one with $\omega>0$ in each interval $j_{sn}<\kappa<j'_{(s+1)n}$. There may also be an intercept for the case $\omega>0$ for $0<\kappa<j'_{1n}$ if $K^2<n(n+1)$, which can be interpreted as a Kelvin wave. The subinertial case can be analysed in a similar manner. Let

$$\Psi(\gamma)=\gamma \mathrm{I}'_n(\gamma)/n\mathrm{I}_n(\gamma)=1+\gamma \mathrm{I}_{n+1}(\gamma)/n\mathrm{I}_n(\gamma), \tag{3.10}$$

so that the dispersion relation (3.6*b*) becomes

$$K/\omega=\pm K/(K^2-\gamma^2)^{1/2}=\Psi(\gamma). \tag{3.11}$$

In this case it is readily shown that only the case $\omega>0$ is possible, and then only if $K^2>n(n+1)$, since now $\Psi(\gamma)$ increases from 1 to ∞ for $0<\gamma<\infty$. A typical set of values is shown in table 1, where for each n we index the modes with $s=\pm1,\pm2,\pm3,\ldots$ according to the magnitude of the roots, and the sign is that of ω. In general, for each $|s|$, $|\omega|$ increases with n, and for each n, $|\omega|$ increases with $|s|$; also, for each fixed n, $|s|$, the negative frequencies are larger in absolute value than the positive frequencies, but converge in absolute value as $|s|$ increases. In the limit of special interest when $K\to\infty$, for the superinertial waves ω scales with K and then the superinertial Poincaré waves are given by $\kappa\approx j'_{sn}$, the zeros of J'_n, indexed by $s=1,2,3,\ldots,$ and so

$$\omega^2\sim K^2+j'^2_{sn}. \tag{3.12}$$

Note that as $K\to\infty$, the frequencies accumulate towards K, that is, in dimensional variables towards the inertial frequency f. However, for the subinertial Kelvin wave, although $\gamma\approx K$, the frequency remains of order unity, given by, from (3.6*b*),

$$\omega\sim n\mathrm{I}_n(K)/\mathrm{I}'_n(K)\sim n,\quad n=1,2,\ldots. \tag{3.13}$$

This is valid when $K^2>n(n+1)$.

3.2. *The initial-value problem and the steady state*

The initial value problem for the nth Fourier mode is the set (3.2*a*), (3.2*b*) and (3.2*c*). This can be solved with Laplace transforms. Note that the mass constraint (2.16) is automatically satisfied by all modes $n\neq0$, and for the mode $n=0$ becomes

$$\int_0^1 \eta_0 r\,\mathrm{d}r=\frac{M}{2\pi}=\int_0^1 \eta_{I0} r\,\mathrm{d}r. \tag{3.14}$$

The solution for each Fourier component consists of a sum of free waves and the steady solution, $\eta_{Sn}(r)$, satisfying the steady form of (3.2*a*) subject to the boundary

https://doi.org/10.1017/jfm.2013.598 Published online by Cambridge University Press

conditions

$$\eta_{Sn} = 0 \quad \text{at } r = 1 \text{ when } n \neq 0, \tag{3.15a}$$

$$\eta_{Snr} = 0 \quad \text{at } r = 1 \text{ when } n = 0. \tag{3.15b}$$

Condition (3.15*a*) follows from (3.2*b*) and condition (3.15*b*) from the zero-circulation condition for flows released from rest, automatically ensuring that η_S satisfies the mass constraint (3.14). The solution for η_{Sn} can be readily expressed in terms of Bessel functions, dropping the Fourier subscript n, as

$$\eta_S = A_n \mathrm{I}_n(Kr) + B_n \mathrm{K}_n(Kr) + K\left\{\mathrm{I}_n(Kr)\int_r^1 \eta_I(\hat{r})\,\mathrm{K}_n(K\hat{r})\,\hat{r}\,\mathrm{d}\hat{r} - \mathrm{K}_n(Kr)\int_r^1 \eta_I(\hat{r})\,\mathrm{I}_n(K\hat{r})\,\hat{r}\,\mathrm{d}\hat{r}\right\}, \tag{3.16}$$

where the constants A_n, B_n are determined by the boundary condition (3.15*a*) or (3.15*b*), and the requirement that the solution be bounded as $r \to 0$. Thus

$$B_n = K\int_0^1 \mathrm{I}_n(Kr)\eta_I r\,\mathrm{d}r \quad (n \geqslant 0), \qquad A_n = \begin{cases} -B_0\mathrm{K}_1(K)/\mathrm{I}_1(K) & n = 0 \\ -B_n\mathrm{K}_n(K)/\mathrm{I}_n(K) & n \geqslant 0. \end{cases} \tag{3.17}$$

Note that in the limit $K \to \infty$, η_S is of order unity. Indeed, except in a boundary layer near $r = 1$ of thickness $a = 1/K$, $\eta_S \approx \eta_I$.

To solve the initial value problem, we introduce $\phi(r, t) = \eta - \eta_S$, the difference between the full solution and the steady-state solution. In the unbounded linear problem ϕ is a transient response that decays at large time due to Poincaré wave radiation. Here, in the bounded domain ϕ gives the Poincaré modes and Kelvin wavefields and is governed by the homogeneous form ($\eta_{In} = 0$) of (3.2*a*) subject to (3.2*b*) and the initial condition

$$\phi = \phi_I = \eta_I - \eta_S, \quad \phi_t = 0 \quad \text{at } t = 0. \tag{3.18}$$

Next we take a Laplace transform

$$\Phi(r, \sigma) = \int_0^\infty \exp(-\sigma t)\phi(r, t)\,\mathrm{d}t, \quad \phi(r, t) = \frac{1}{2\pi\mathrm{i}}\int_C \exp(\sigma t)\Phi(r, \sigma)\,\mathrm{d}\sigma, \tag{3.19}$$

where C is a contour in $\mathrm{Re}\{\sigma\} > 0$ from $\epsilon - \mathrm{i}\infty$ to $\epsilon + \mathrm{i}\infty$, where $\epsilon > 0$ is chosen so that all singularities of Φ lie to the left of C. Then equations (3.2*a*), (3.2*b*) and (3.18) become

$$\Phi_{rr} + (1/r)\Phi_r - (n^2/r^2)\Phi - \sigma^2\Phi - K^2\Phi = -\sigma\phi_I, \tag{3.20a}$$

$$\sigma r\Phi_r - \mathrm{i}nK\Phi = \phi_{Ir} \quad \text{on } r = 1. \tag{3.20b}$$

This ordinary differential equation boundary value problem can now be solved explicitly,

$$\Phi = C_n\mathrm{I}_n(\gamma r) + D_n\mathrm{K}_n(\gamma r) - (\sigma/\gamma)\left\{\mathrm{I}_n(\gamma r)\int_r^1 \phi_I(\hat{r})\mathrm{K}_n(\gamma\hat{r})\,\hat{r}\,\mathrm{d}\hat{r} - \mathrm{K}_n(\gamma r)\int_r^1 \phi_I(\hat{r})\,\mathrm{I}_n(\gamma\hat{r})\,\hat{r}\,\mathrm{d}\hat{r}\right\}, \tag{3.21}$$

https://doi.org/10.1017/jfm.2013.598 Published online by Cambridge University Press

where $\gamma^2 = \sigma^2 + K^2$ and the constants C_n, D_n are determined by the boundary conditions,

$$C_n[\sigma\gamma \mathrm{I}_n'(\gamma) - \mathrm{i}nK\mathrm{I}_n(\gamma)] + D_n[\sigma\gamma \mathrm{K}_n'(\gamma) - \mathrm{i}nK\mathrm{K}_n(\gamma)] = \phi_{Ir}(1), \tag{3.22a}$$

$$D_n = -\frac{\sigma}{\gamma}\int_0^1 \mathrm{I}_n(\gamma r)\,\phi_{Ir}\, r\,\mathrm{d}r. \tag{3.22b}$$

As a function of σ, $\Phi(\sigma, r)$ has poles at $\sigma = -\mathrm{i}\omega$ where

$$\omega\gamma \mathrm{I}_n'(\gamma) + nK\mathrm{I}_n(\gamma) = 0, \quad \gamma^2 = K^2 - \omega^2. \tag{3.23}$$

The frequencies so determined are precisely those of the free waves determined in § 3.1, see (3.5) and (3.6*b*) where $\gamma = \mathrm{i}\kappa$, $\kappa^2 = \omega^2 - K^2$ in the former case. In the limit of interest when $K \to \infty$, the Poincaré waves have high frequencies ω scaling with K (as in § 3.1) and have amplitudes of order $a = 1/K$, most readily inferred directly from (3.20*a*). On the other hand, in this same limit, the Kelvin wave has an order-unity frequency, an order-unity amplitude and is confined to the outer boundary to within a layer of order a. Hence, the complete solution then consists essentially of simply the steady solution, adjusted at the boundary by a Kelvin wave.

3.3. *Numerical results*

Although the expressions (3.19) and (3.21) formally provide an explicit solution for ϕ, in general the integrals involving ϕ_I are not straightforward to evaluate: it is simpler to solve (3.2*a*), (3.2*b*) and (3.2*c*) directly by high-accuracy spectral discretization. Here (3.2*a*), (3.2*b*) and (3.2*c*) are discretized with 128 Chebyshev points over $-1 \leqslant x \leqslant 1$, following Fornberg (1995), and using an appropriate parity condition to extend the solution to negative r. This extension avoids stringent CFL conditions at the origin and automatically copes with the polar coordinate singularity there. The spatially discretized equations were integrated forward in time with an Adams–Bashforth method. Integrations at higher resolutions differed by less than 10^{-8} from those presented here. For small K (large a) when the Rossby radius is large compared with the basin diameter, the rotational effects are weak and the flow evolves similarly to non-rotating flow. Hence, the results presented here are for $a = 0.05$, $K = 20$, when the Rossby radius is one-twentieth of the basin radius, the non-dimensional inertial period is approximately $\pi/10$, and the Kelvin wave cycles the basin in a non-dimensional time of approximately 2π.

3.3.1. *Case 1. Axisymmetric flow: $n = 0$.*

Consider the top-hat initial condition

$$\eta_{I0} = -\tanh[(r - r_0)/r_w], \tag{3.24}$$

for a downward step of height 2 centred at radius r_0 (taken as 0.5 here and below) and of width r_w (taken as 0.025 here and below). Figure 3 shows this initial condition and the steady adjusted solution η_S where the steep initial step has been smoothed by a layer of thickness of order $a = 1/K$. Figure 4 shows a snapshot at $t = 10$ of the surface perturbation η for this initial profile. As the flow is axisymmetric no Kelvin wave is excited in the evolution and, for the small value of the Rossby radius a here, the Poincaré waves have amplitudes, wavelengths and non-dimensional periods of order a. The average surface displacement over the interval $0 \leqslant t \leqslant 10$ is graphically indistinguishable from η_S. The effect of the Poincaré waves averages to zero over sufficiently many inertial periods. Figure 5(*a*) shows the variation with K of the fraction of the initial state energy, computed from (2.27*b*), in the geostrophic

https://doi.org/10.1017/jfm.2013.598 Published online by Cambridge University Press

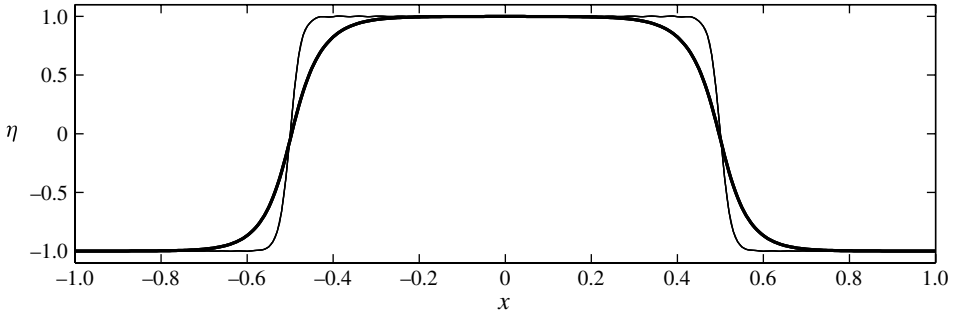


FIGURE 3. A cross-section along the line $y = 0$ of the initial surface perturbation η_{I0} for an axisymmetric ($n = 0$) top-hat profile (thin line) and the steady adjusted solution η_S (bold line). Here $a = 0.05$ so the Rossby radius is one-twentieth the basin radius. The steep initial step has been smoothed by a layer of thickness of order a.

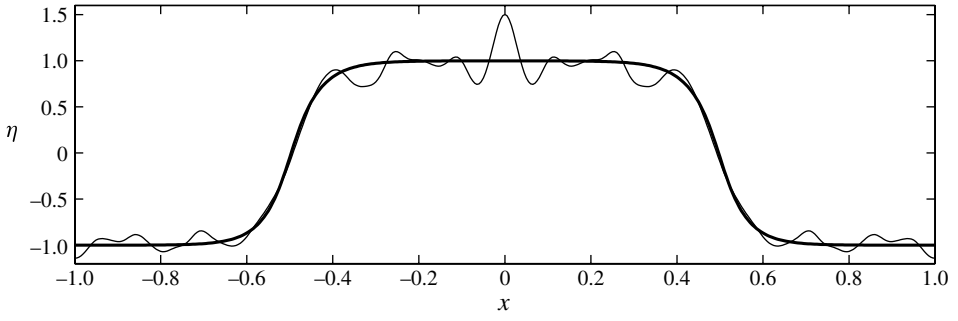


FIGURE 4. A snapshot at $t = 10$ along the line $y = 0$ of the surface perturbation η (thin line) for the top-hat profile of figure 3. As in figure 3, the bold line gives the steady adjusted solution η_S. There is no Kelvin wave in the evolution and the Poincaré waves have amplitudes, wavelengths and non-dimensional periods of order a. The average surface displacement over the interval $0 \leqslant t \leqslant 10$ is graphically indistinguishable from η_S. An animated version of the evolution of the surface perturbation here is available in the supplementary material (http://dx.doi.org/10.1017/jfm.2013.598).

and Poincaré modes for the initial state (3.24). The kinetic energy of the geostrophic mode reaches a maximum at $K \approx 4$ with the flow at large K dominated by the surface deformation of the adjusted mode and the contributions from the Poincaré waves and geostrophic kinetic energy negligible.

3.3.2. *Case 2. Non-axisymmetric single-azimuth flow: $n = 1$.*
Case 2a. A stepped profile

Consider azimuthal dependence $n = 1$, with the initial radial profile

$$\eta_{I1} = 0.5\{1 + \tanh[(r - r_0)/r_w]\}, \tag{3.25}$$

giving an upward step of height 1 (at $r = r_0$ and of width r_w, as above). Figure 6 shows this initial condition and the steady adjusted solution η_S where the steep initial step has been smoothed by layers of thickness of order a. A second layer of thickness a at the boundary adjusts the interior steady solution to the zero-displacement condition at the wall, effectively the condition that there can be no

https://doi.org/10.1017/jfm.2013.598 Published online by Cambridge University Press

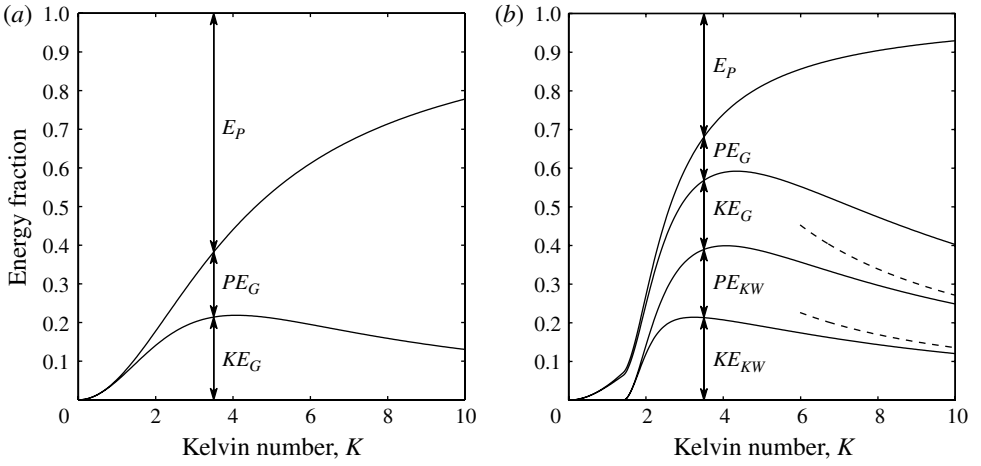


FIGURE 5. The variation with K of the fraction of the initial state energy in the kinetic and potential energy of the geostrophic mode (KE_G, PE_G) and the Kelvin wave (KE_{KW}, PE_{KW}) and the total energy of the Poincaré wavefield (E_P) for the axisymmetric initial profile (3.24) (*a*) and the azimuthal mode-one profile (3.25) (*b*). The dashed curves give the values of the Kelvin wave kinetic and total energy from the large K asymptotic form (3.26).

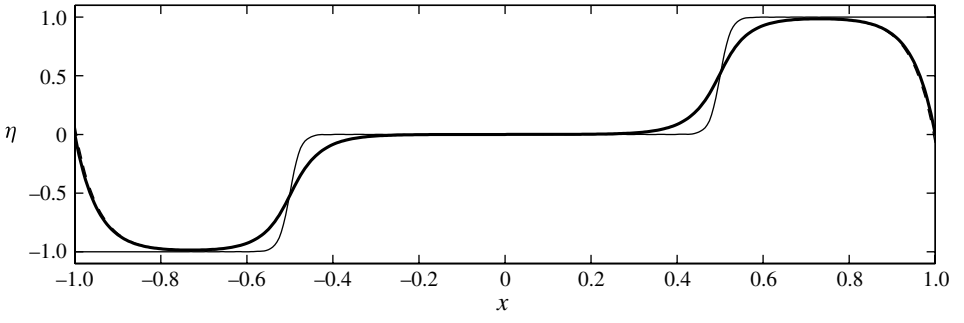


FIGURE 6. A cross-section along the line $y = 0$ of the initial surface perturbation η_{I1} for an azimuth one ($n = 1$) profile (thin line) and the steady adjusted solution η_S (bold line). As in figure 3, $a = 0.05$ so the Rossby radius is one-twentieth the basin radius. The steep initial step has been smoothed by layers of thickness of order a. A second layer of thickness a at the boundary adjusts the interior steady solution to the zero-displacement condition at the wall.

tangential gradient in the steady solution at a solid boundary and consequently no normal component of velocity there. Figure 7 shows a snapshot at $t = 10$ of the surface perturbation η for this initial profile. Here the flow is not axisymmetric so a single Kelvin wave mode is excited in the evolution. The wave has amplitude of the order of the difference between the initial and steady states at the wall, period of order 2π and is confined to within a distance of order the Rossby radius of the boundary. This can be simply modelled by adding the appropriate Kelvin wave mode of this amplitude to the steady solution as shown by the dashed line in figure 7. For the small value of the Rossby radius a here it is sufficient to use the asymptotic expression for

https://doi.org/10.1017/jfm.2013.598 Published online by Cambridge University Press

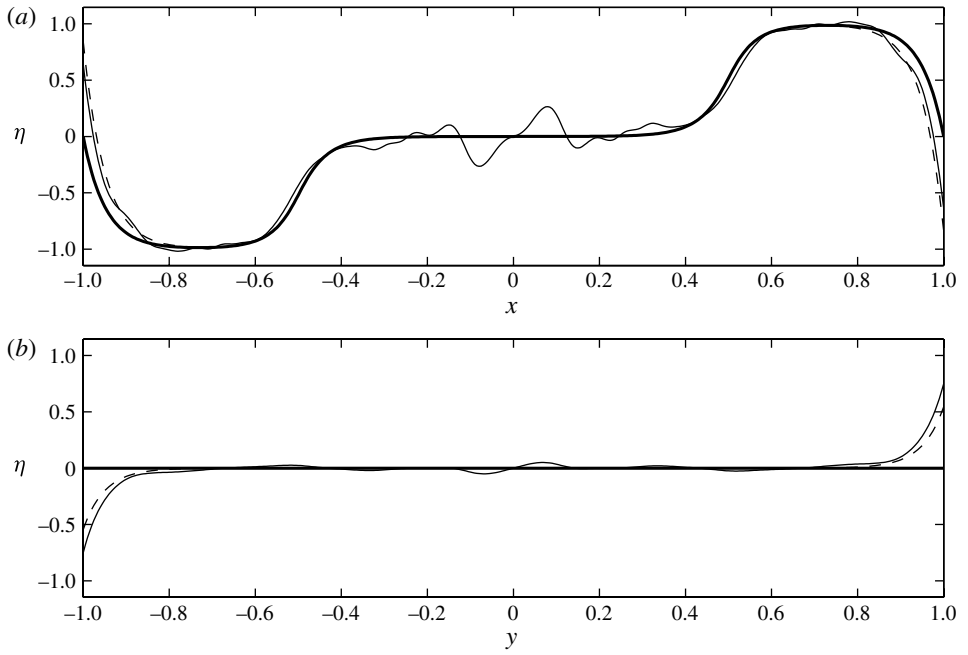


FIGURE 7. Snapshots at $t = 10$ along the lines $y = 0$ (a) and $x = 0$ (b) of the surface perturbation η (thin line) for the $n = 1$ profile of figure 6. As in figure 6, the bold line gives the steady adjusted solution η_S. The dashed line gives the sum of the steady solution and the single Kelvin wave mode, with period of order 2π and confined to within a distance of order the Rossby radius of the boundary. The Poincaré waves have amplitudes, wavelengths and non-dimensional periods of order a. An animated version of the evolution of the surface perturbation here and a movie of the two-dimensional evolution are available in the supplementary material (http://dx.doi.org/10.1017/jfm.2013.598).

the Bessel function to give the simple Kelvin wave term

$$\eta_K = \eta_{I1}(1)\exp[-K(1-r)]\cos(\theta - t). \tag{3.26}$$

Again, for the small value of the Rossby radius a here, the Poincaré waves have amplitudes, wavelengths and non-dimensional periods of order a, making up the small difference between the dashed and solid lines in figure 7. The surface displacement averaged over times long compared with the inertial period $2\pi/a$, but short or comparable with the Kelvin wave period 2π, is indistinguishable from the combined sum of steady and Kelvin wave components. The surface displacement averaged over times long compared to the Kelvin wave period is given simply by the steady component η_S. Figure 5(b) shows the variation with K of the energy in the modes for the initial state (3.25), computed from (2.27b), (2.28) and (2.32). For motion in a circular domain the wave norm is particularly simple as the mode can be taken as purely real so the Jacobian term in (2.28) vanishes; however, it appears that the circle is the unique closed domain with this property. As for condition (3.24), the kinetic energy of the geostrophic mode reaches a maximum at $K \approx 4$ with the flow at large K dominated by the surface deformation of the adjusted mode and the contributions from the Poincaré waves and geostrophic kinetic energy negligible. However, in addition once $K > 2^{1/2}$ (see § 3.1), a Kelvin wave is also present. The precise division of energy

https://doi.org/10.1017/jfm.2013.598 Published online by Cambridge University Press

among the component modes is highly sensitive to the initial conditions depending as it does on the projection (2.32) onto the free modes. Thus, in the example of a linearly sloping surface, solved explicitly below as Case 2*b*, from Stocker & Imberger (2003), the geostrophic component vanishes at large K as its inner product with the initial condition becomes vanishingly small. The dashed lines in figure 5 give the components of Kelvin wave energy determined from the asymptotic form (3.26) showing that (3.26) estimates the components to within 5 % by $K \approx 6$, becoming progressively more accurate with increasing K.

Case 2b. A uniformly sloping profile: closed form solution

The initial value problem considered by Stocker & Imberger (2003) corresponds to the azimuthal dependence $n = 1$ with an initial radial profile giving a uniformly sloping initial surface displacement, $\eta_{I1} = r$. The interior flow is already in geostrophic balance and the solution can be obtained explicitly without requiring the steady solution. Write $\psi(r, t) = \eta(r, t) - r$ and introduce the Laplace transform, $\Psi(r, \sigma)$. Then Ψ satisfies the homogeneous form ($\phi_I = 0$) of (3.20*a*) subject to

$$\sigma r \Psi_r + \mathrm{i}K\Psi = \mathrm{i}K \quad \text{on } r = 1, \tag{3.27}$$

giving

$$\begin{aligned} \Psi(r, \sigma) &= \mathrm{i}K\mathrm{I}_1(\gamma r)/[\sigma\gamma \mathrm{I}_1'(\gamma) + \mathrm{i}K\mathrm{I}_1(\gamma)] \\ &= \mathrm{i}K\mathrm{I}_1(\gamma r)/[\sigma\gamma \mathrm{I}_0(\gamma) + (\mathrm{i}K - \sigma)\mathrm{I}_1(\gamma)], \end{aligned} \tag{3.28}$$

where $\gamma = (\sigma^2 + K^2)^{1/2}$. Summing the residues at the zeros of the denominator in the Bromwich integral gives $\psi(r, t)$. In the limit of large K (small a) only the residue corresponding to the Kelvin wave remains non-zero, giving the result (3.26), where here $\eta_{I1}(1) = 1$.

3.4. *The large K limit*

Example 2*b* shows that in the circular domain in the small a, large $K = 1/a$ limit the leading order (in a) response for any n consists of the steady response plus a mode n Kelvin wave. For more general initial conditions the leading order response consists of the steady state response plus a superposition of boundary-confined Kelvin waves. Moreover, the average over time periods that are long compared with the Poincaré waves periods is closely estimated by this combined response. Now the uniformly first-order (in a) steady solution satisfies (2.14) subject to the boundary conditions (2.15) as noted in § 2 and since a is small, the form of the steady solution follows straightforwardly. Away from the boundary, and outside regions where the initial elevation varies on scales of order a or less, $\eta_S = \eta_I$ and the initial elevation is unchanged. Rapidly varying regions of η_0 are smoothed by layers of thickness a, and a similar layer of thickness a can be present around the boundary to satisfy the circulation constraint. The remainder of the response is the Kelvin wave response, confined to within a distance a from the boundary. Thus we introduce the scaled normal coordinate $\xi = K(1 - r) \geqslant 0$. Then the leading-order Kelvin wave response, $\eta_K(\xi, \theta, t)$ satisfies

$$\eta_{K\xi\xi} - \eta_K = 0, \quad \xi > 0, \tag{3.29}$$

subject to

$$\eta_{K\xi t} - \eta_{K\theta} = 0, \quad \text{on } \xi = 0, \ t > 0, \tag{3.30a}$$

$$\eta_K(1, \theta) + \eta_S(1, \theta) = \eta_I(1, \theta) \quad \text{on } \xi = 0, \ t = 0, \tag{3.30b}$$

https://doi.org/10.1017/jfm.2013.598 Published online by Cambridge University Press

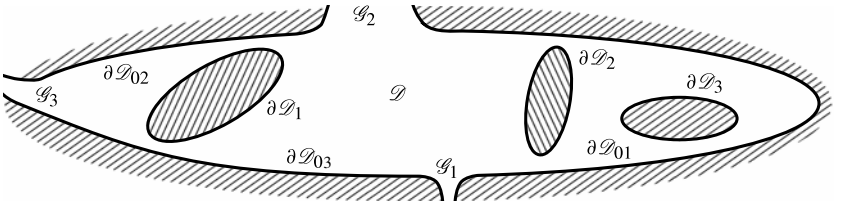


FIGURE 8. The basin $\mathscr{D}$ with islands with boundaries $\partial\mathscr{D}_i$ $(i = 1, 2, \ldots)$ and outer boundary $\partial\mathscr{D}_0$ split into sections $\partial\mathscr{D}_{0j}$ $(j = 1, 2, \ldots)$ by gaps $\mathscr{G}_j$.

with solution

$$\eta_K(\xi, \theta, t) = F(\theta + t)\exp(\xi), \quad F(\theta) = \eta_I(1, \theta) - \eta_S(1, \theta) = \eta_I(1, \theta) - \alpha_0. \tag{3.31}$$

The departure of the initial surface displacement at the wall from its long-term average (α_0) propagates at the constant dimensional longwave speed c around the wall (with the wall to the right, as expected) without change of form.

4. Adjustment in arbitrary domains for large K

The generalization of the results of § 3 for large K to the arbitrary basin with islands of § 2 follows immediately. Provided that the boundary geometry is slowly varying on the (small) scale of the Rossby radius, so Kelvin wave energy is not scattered into Poincaré waves, the leading-order (in a) flow can be expressed as the sum of steady, η_S, and Kelvin wave, η_K, components where the steady component satisfies (2.14) throughout $\mathscr{D}$ subject to the boundary conditions (2.15). The Kelvin wave component satisfies (3.29) at each $\partial\mathscr{D}_i$ provided that ξ is generalized to be the normal distance, scaled on a, measured inwards from the relevant boundary. The boundary conditions at each $\partial\mathscr{D}_i$ become

$$\eta^{(i)}_{K\xi t} + \eta^{(i)}_{Ks} = 0 \quad \text{on } \partial\mathscr{D}_i, \ t > 0, \tag{4.1a}$$

$$\eta^{(i)}_K = \eta_I - \alpha_i = k_i(s) \text{ (say)} \quad \text{on } \partial\mathscr{D}_i, \ t = 0, \tag{4.1b}$$

where s is the arclength (measured anticlockwise around $\partial\mathscr{D}_0$ and clockwise around $\partial\mathscr{D}_i$, $i = 1, 2, \ldots$). The solution $\eta^{(i)}_K$ is thus

$$\eta^{(i)}_K(\xi, s, t) = k_i(s - t)\exp(\xi), \tag{4.2}$$

with, again, the departure of the initial surface displacement on each $\partial\mathscr{D}$ from its long-term average (α_i) propagating around the boundary at (dimensional) speed c with the wall to the right and without change of form.

In practice basins may not be completely closed and small gaps may be present in the outer boundary. This certainly applies to the Arctic Ocean, but is also usually the case even for large lakes. Figure 8 shows a typical basin with gaps $\mathscr{G}_j$, $(j = 1, 2, \ldots)$ breaking the outer boundary $\partial\mathscr{D}_0$ into sections $\partial\mathscr{D}_{0j}$ (with $\partial\mathscr{D}_{0j}$ extending clockwise from $\mathscr{G}_j$). The analysis above extends directly provided allowance is made for the absence of a circulation condition on $\partial\mathscr{D}_0$. If all gaps are wider than the relevant Rossby radius then the steady elevation α_{0j} on $\partial\mathscr{D}_{0j}$ is given simply by the upstream elevation of the corresponding boundary of gap $\mathscr{G}_j$, and the steady component η_S satisfies (2.14) subject to the boundary conditions (2.15), but taking the values α_{0j} on each section $\partial\mathscr{D}_{0j}$. The Kelvin wave on each section is driven, as above, by

https://doi.org/10.1017/jfm.2013.598 Published online by Cambridge University Press

the difference between the initial elevation and the average α_{0j} but, for the broken outer boundary, rapidly propagates out of the flow domain. If any gap $\mathscr{G}_j$ is narrower than the Rossby radius, then the determination of the constant steady elevation on $\partial\mathscr{D}_{0j}$ is unchanged if $\alpha_{0j-1} = \alpha_{0j}$ (which is the case if the adjustment occurs in the basin rather than between gaps with different initial surface elevations) so there is no incompatibility in the steady elevations on either boundary of $\mathscr{G}_j$, but otherwise depends on the details of the gap geometry.

5. Discussion

Prompted by recent discussions of motion in the Arctic Ocean we have considered the general problem of adjustment in an arbitrary basin with islands. The evolving flow consists of a steady adjusted geostrophic component and free waves. The amplitude of both components of the solution follow directly by projection from the initial conditions and thus depend sensitively on them. There appears to be no completeness result for these expansions and thus we present the solution for adjustment from arbitrary initial conditions in a circular domain, where the evolution, the geostrophic mode and the Kelvin and Poincaré modes can be identified and found explicitly. For general domains, obtaining the free modes is not straightforward analytically with Goldstein (1929) giving an expansion method for an elliptic basin but remaining progress being numerical (Platzman 1972). Distinguishing between boundary-trapped and basin motions is also problematic in general, as illustrated by the vanishing of Kelvin wave modes in the circular domain when $K < 2^{1/2}$. Guided by this and the observation that the first baroclinic deformation in the Canada Basin is of the order of 10 km (Timmermans *et al.* 2010), we focus on baroclinic vertical modes when the non-dimensional Rossby radius $a = 1/K$ is small. The boundary then has little effect on the interior solution and, apart from the presence of small-amplitude, $O(a)$, Poincaré waves, conservation of potential vorticity implies that the steady interior solution for the height field is hardly changed from the initial state. Since this applies to each vertical mode, if the Rossby radii of the modes are small (in fact, it is sufficient for the Rossby radius of the lowest vertical mode present to be small) and interior potential vorticity smooth then it is unnecessary to separate the potential vorticity into vertical modes to follow the interior adjustment. Of course, this final interior steady potential vorticity distribution, being in geostrophic balance, will be accompanied by a geostrophic velocity field generated during the adjustment process, but this velocity follows immediately from the usual geostrophic relations for the horizontal velocities. Near the boundary a superposition of Kelvin waves decaying towards the interior over distances of order the Rossby radius carry the deviation of the initial surface displacement from its average around the boundary without change of form. We suggest that during adjustment gaps and islands have a large (order unity) local effect but that for small a this is confined to an unsteady region of width $O(a)$ close to the basin boundary and islands.

Two unrelated nonlinear effects can appear in the evolution. First, the Kelvin waves propagating around the boundary can break even at small amplitude if the initial tangential gradients are sufficiently large. Second, with larger initial perturbations the velocities engendered can be sufficiently large that the advection of potential vorticity can be important. Potential vorticity advection during adjustment in a rotating channel is analysed using contour dynamics in Hermann, Rhines & Johnson (1989) but as their channel geometry is open all wave energy escapes leaving a slow vorticity evolution. Wake *et al.* (2007) compare their experimental observations with contour dynamics

https://doi.org/10.1017/jfm.2013.598 Published online by Cambridge University Press

simulations but, as with Hermann *et al.* (1989), the limit used precludes discussion of wave–vortex interactions. These effects in completely closed domains will be examined in more detail elsewhere.

When islands are present energy from the initial state can be retained in Kelvin wave modes cycling the islands in addition to the geostrophic mode even when the entire flow region is unbounded and Poincaré wave energy escapes to infinity, provided that a is sufficiently small for spatially evanescent modes to exist. An example related to this is the Southern Mode, an observed periodic variation in the transport of the Antarctic Circumpolar Current that is highly correlated with both the wind stress (Hughes, Meredith & Heywood 1999), and the fluctuations in the transport through the Drake Passage (Meredith *et al.* 2004). Observations (Peterson 1988) show the motion is predominantly barotropic at time scales of less than a year. Thus, a simple model is given by writing (2.11) in terms of η as

$$\eta_{ttt} - \nabla^2\eta_t + K^2\eta_t = -K^2\mathscr{F}(x,y)\cos(\omega_F t), \tag{5.1}$$

where the right-hand side gives the periodic generation of vorticity by wind stress curl, with specified frequency ω_F, spatial distribution $\mathscr{F}(x,y)$ and scaled to be a time rate of change of sea-surface elevation. For the simple domain exterior to the circle $r=1$, the forced response can be expressed in terms of Fourier modes as in (3.1), with each mode η_{Fn} satisfying (3.2*a*) with right-hand side $(K^2/\omega_F)\mathscr{F}_n(r)\sin(\omega_F t)$ and boundary condition (3.2*b*). If ω_F corresponds to a Kelvin wave mode of the system, and the wind stress has non-zero projection on that mode, then the linear inviscid response would grow without limit. Here we restrict attention to axisymmetric forcing and since, as in § 3.1, there is no axisymmetric Kelvin wave, the linear response is finite for all ω_F. Then (3.2*b*) reduces to (3.15*b*), giving the solution, bounded at large r,

$$\begin{aligned}\eta_{F0}(r,t) = {}& (K/\omega_F)\mathrm{I}_0(\gamma_F r)\sin(\omega_F t)\int_r^\infty \mathscr{F}_0(\hat{r})\mathrm{K}_0(\gamma_F\hat{r})\hat{r}\,\mathrm{d}\hat{r}\\ &+ (K/\omega_F)\mathrm{K}_0(\gamma_F r)\sin(\omega_F t)\left\{\int_1^r \mathscr{F}_0(\hat{r})\mathrm{I}_0(\gamma_F\hat{r})\,\hat{r}\,\mathrm{d}\hat{r}\right.\\ &\left.+ [\mathrm{I}_1(\gamma_F)/\mathrm{K}_1(\gamma_F)]\int_1^\infty \mathscr{F}_0(\hat{r})\mathrm{K}_0(\gamma_F\hat{r})\,\hat{r}\,\mathrm{d}\hat{r}\right\},\end{aligned} \tag{5.2}$$

where $\gamma_F^2 = K^2 - \omega_F^2$. Evaluating (5.2) on $r=1$ immediately gives the surface elevation at the coast

$$\begin{aligned}\eta_{F0}(0,t) = {}& (K/\omega_F)\sin(\omega_F t)\{\mathrm{I}_0(\gamma_F) + \mathrm{K}_0(\gamma_F)[\mathrm{I}_1(\gamma_F)/\mathrm{K}_1(\gamma_F)]\}\\ &\times\int_1^\infty \mathscr{F}_0(\hat{r})\mathrm{K}_0(\gamma_F\hat{r})\,\hat{r}\,\mathrm{d}\hat{r},\end{aligned} \tag{5.3}$$

a non-dimensional estimate for the fluctuations in volume flux. The inclusion of realistic topographic depth variation $H(x,y)$ is straightforward (Proudman 1929), although care must be taken if f/H contours close locally rather than cycle the entire boundary (Greenspan 1965). Kusahara & Ohshima (2009) give a rigid-lid, low-frequency one-dimensional solution including topography for one specific forcing and conclude that the trapping of the sea-level disturbance at the coast is due to the topographic gradient in their example. Solution (5.2) shows that this is not always so and that the exponential decay of the forced mode response, particularly for large Kelvin number, also confines the disturbance close to the coast and the integral in (5.3) shows that it is the wind stress forcing nearest the coast that makes the largest

https://doi.org/10.1017/jfm.2013.598 Published online by Cambridge University Press

contribution to the surface displacement there and thus the volume flux estimate. The forced mode here is not a free mode of the system: the full equation (5.1) admits no finite-energy, time-dependent, axisymmetric free mode external to the circle. The free mode of Hughes *et al.* (1999) corresponds to the geostrophic mode which is steady here on both the inertial and Kelvin wave time scales. The geostrophic mode will vary on much longer time scales, although Hughes *et al.* (1999) conclude from model results that it is not the dominant response, reinforced by Weijer & Gille (2005) who note that less than 10 % of the response they compute is ascribable to a free mode. Both Hughes *et al.* (1999) and Weijer & Gille (2005) point out the difficulty that simple models such as (5.1) give a response that is $\pi/2$ out of phase with the winds and that this phase difference is not found in the observations or numerical modelling. This example is given here and described in terms of the significant body of knowledge of the Southern Mode, as it appears possible that similar forced steady and periodic modes (and baroclinic modes in particular) driven directly by the wind stress curl, with round-island circulations strengths determined by the wind, are likely near the islands and coasts of the Arctic Ocean perhaps in the form of the topographic waves described by Timmermans *et al.* (2010).

Acknowledgement

We are indebted to Professor C. Hughes for providing us with an extended version of his contribution to Meredith *et al.* (2011).

Supplementary movies

Supplementary movies are available at http://dx.doi.org/10.1017/jfm.2013.598.

REFERENCES

FORNBERG, B. 1995 A pseudospectral approach for polar and spherical geometries. *SIAM J. Sci. Comput.* **16**, 1071–1081.

GILL, A. E. 1976 Adjustment under gravity in a rotating channel. *J. Fluid Mech.* **77**, 603–621.

GILL, A. E. 1982 *Atmosphere–Ocean Dynamics*. Academic.

GOLDSTEIN, S. 1929 Tidal motion in a rotating elliptic basin of constant depth. *Mon. Not. R. Astron. Soc. Geophys. Suppl.* **2**, 213–231.

GOMEZ-GIRALDO, A., IMBERGER, J. & ANTENUCCI, J. P. 2006 Spatial structure of the dominant basin-scale internal waves in Lake Kinneret. *Limnol. Oceanogr.* **51**, 229–246.

GREENSPAN, H. P. 1965 On the general theory of contained rotating fluid motions. *J. Fluid Mech.* **22**, 449–462.

HERMANN, A. J., RHINES, P. B. & JOHNSON, E. R. 1989 Nonlinear Rossby adjustment in a channel – beyond Kelvin waves. *J. Fluid Mech.* **205**, 469–502.

HUGHES, C. W., MEREDITH, M. P. & HEYWOOD, K. J. 1999 Wind-driven transport fluctuations through Drake Passage: a southern mode. *J. Phys. Oceanogr.* **29**, 1971–1992.

JOHNSON, E. R. 1989 Scattering of shelf waves by islands. *J. Phys. Oceanogr.* **19**, 1311–1316.

KAMENKOVICH, V. M. 1961 The integration of the marine current theory equations in multiply connected regions. *Dokl. – Acad. Sci. USSR Earth Sci. Sec.* **138**, 629–631.

KUSAHARA, K. & OHSHIMA, K. I. 2009 Dynamics of the wind-driven sea level variation around Antarctica. *J. Phys. Oceanogr.* **39**, 658–674.

LAMB, H. 1932 *Hydrodynamics*. Cambridge University Press.

LIN, C. C. 1941 On the motion of vortices in two-dimensions. I. Existence of the Kirchhoff–Routh function. *Proc. Natl Acad. Sci.* **27**, 570–577.

LUNEVA, M. V., WILLMOTT, A. J. & MAQUEDA, M. A. M. 2012 Geostrophic adjustment problems in a polar basin. *Atmos.-Ocean* **50**, 134–155.

https://doi.org/10.1017/jfm.2013.598 Published online by Cambridge University Press

MEREDITH, M. P., WOODWORTH, P. L., CHERESKIN, T. K., MARSHALL, D. P., ALLISON, L. C., BIGG, G. R., DONOHUE, K., HEYWOOD, K. J., HUGHES, C. W., HIBBERT, A., HOGG, A. MCC., JOHNSON, H. L., JULLION, L., KING, B. A., LEACH, H., LENN, Y.-D., MORALES MAQUEDA, M. A., MUNDAY, D. R., NAVEIRA GARABATO, A. C., PROVOST, C., SALLÉE, J.-B. & SPRINTALL, J. 2011 Sustained monitoring of the southern ocean at Drake Passage: past achievements and future priorities. *Rev. Geophys.* **49**, RG4005.

MEREDITH, M. P., WOODWORTH, P. L., HUGHES, C. W. & STEPANOV, V. 2004 Changes in the ocean transport through Drake Passage during the 1980s and 1990s, forced by changes in the Southern Annular Mode. *Geophys. Res. Lett.* **31**, L21305.

PETERSON, R. G. 1988 On the transport of the Antarctic Circumpolar Current through Drake Passage and its relation to wind. *J. Geophys. Res.-Oceans* **93**, 13993–14004.

PLATZMAN, G. W. 1972 Two-dimensional free oscillations in natural basins. *J. Phys. Oceanogr.* **2**, 117–138.

PROUDMAN, J. 1929 On a general expansion in the theory of the tides. *Proc. Lond. Math. Soc.* **29**, 527–536.

RHINES, P. B. 1969 Slow oscillations in an ocean of varying depth. 2. Islands and seamounts. *J. Fluid Mech.* **37**, 191–205.

ROSSBY, C. G. 1938 On the mutual adjustment of pressure and velocity distributions in certain simple current systems, II. *J. Mar. Res.* **1**, 239–263.

STOCKER, R. & IMBERGER, J. 2003 Energy partitioning and horizontal dispersion in the surface layer of a stratified lake. *J. Phys. Ocean.* **33**, 512–529.

TIMMERMANS, M. L., RAINVILLE, L., THOMAS, L. & PROSHUTINSKY, A. 2010 Moored observations of bottom-intensified motions in the deep Canada Basin, Arctic Ocean. *J. Mar. Res.* **68**, 625–641.

WAKE, G. W., HOPFINGER, E. J. & IVEY, G. N. 2007 Experimental study on resonantly forced interfacial waves in a stratified circular cylindrical basin. *J. Fluid Mech.* **582**, 203–222.

WAKE, G. W., IVEY, G. N., IMBERGER, J. & MCDONALD, N. R. 2005 The temporal evolution of a geostrophic flow in a rotating stratified basin. *Dyn. Atmos. Oceans* **39**, 189–210.

WAKE, G. W., IVEY, G. N., IMBERGER, J., MCDONALD, N. R. & STOCKER, R. 2004 Baroclinic adjustment in a rotating circular basin. *J. Fluid Mech.* **515**, 63–86.

WEIJER, W. & GILLE, S. T. 2005 Adjustment of the Southern Ocean to wind forcing on synoptic time scales. *J. Phys. Oceanogr.* **35**, 2076–2089.

https://doi.org/10.1017/jfm.2013.598 Published online by Cambridge University Press